

## Final Technical Report

1. Award Number: G14AP00048 and G14AP00053
  
2. Title of Award: Cosmogenic and OSL Dating for Determining Slip Rates of Normal Faults Near Reno: Collaborative Research with University of Nevada, Reno and University of Cincinnati
  
3. Authors: Steven G. Wesnousky<sup>1</sup>  
Lewis A. Owen<sup>2</sup>  
<sup>1</sup> Center for Neotectonic Studies and Seismological Laboratory, 1664 North Virginia Street, University of Nevada, Reno, 89557.  
wesnousky@unr.edu  
<sup>2</sup> Dept of Geology, University of Cincinnati, PO Box 210013, Cincinnati, OH, 45221.  
[Lewis.Owen@uc.edu](mailto:Lewis.Owen@uc.edu)
  
4. Principal Investigators: Steven G. Wesnousky<sup>1</sup> and Lewis A. Owen<sup>2</sup>
  
5. Term of Award: June 1, 2014 – Aug 31, 2015

## **Abstract.**

The Reno-Carson City urban corridor is located in the northern Walker Lane. Geodesy shows that the Walker Lane is currently accommodating 5-6 mm/yr of right-lateral shear. USGS National Seismic Hazard Maps assume that the entirety of the geodetic signal is released as seismic moment and thus contributes to the level of seismic hazard across the region. A recently published study of the region, by one of the PIs and his colleagues (Wesnousky et al. 2012), indicates that the distribution, sense of slip, and slip rate of major faults in the Northern Walker Lane cannot explain the geodetic signal observed across the region. The assumption that all geodetically observed shear across the area is recorded by earthquake displacements thus may be flawed and the level of seismic hazard in the region significantly overestimated. Understanding the disparity is critical to development of seismic hazard methodologies in general and the Reno-Carson urban corridor in particular. Towards examining the cause of the disparity and contributing information for seismic hazard analysis in the area, we requested funds to conduct fault slip rate studies on two of the main range-bounding normal faults that comprise the northern Walker Lane. The two faults are located in Smith and Mason Valleys, Nevada. Toward that end, we collected and conducted  $^{10}\text{Be}$  TCN surface dating of boulders and depth profiles on two fans offset along the respective range bounding faults of Smith and Mason Valley. We find the preferred values of fault slip rate and extension are .112 mm/yr and 0.056 mm/yr along the bounding normal fault that strikes along the western edge of Mason Valley. In Smith Valley, preferred values of fault slip rate and extension are estimated at 0.68 mm/yr and 0.58 mm/yr, respectively.

# Report

## Introduction

The urban Reno corridor sits within the Northern Walker Lane as do the faults of Smith and Mason valleys (Figure 1). The Northern Walker Lane is currently the locus of 5-6 mm/yr of right-lateral shear strain. It is assumed in current USGS National Seismic Hazard Maps that the entirety of the strain signal is released as seismic moment (the formula of Kostrov is used to convert the portion of geodetic strain rate that is not assigned to major faults to seismic moment rate and thus earthquakes between the faults). A recent study shows the distribution, sense of slip, and slip rate of major faults in the Northern Walker Lane cannot explain the geodetic signal observed across the region (Wesnousky et al. 2012). The result has a number of very important implications. The assumption that all geodetically observed shear across the area will be recorded by earthquake displacements may be flawed. If so, the level of seismic hazard in the region may be significantly overestimated. And the actual level of seismic hazard is probably better reflected in the assumption that the potential size and recurrence time of earthquakes is a respective function of the lengths and rates of slip on the major faults in the region. Toward confirming whether or not the discrepancy between geodetic and geologic rates is indeed real, we collected and conducted  $^{10}\text{Be}$  TCN surface dating of boulders and depth profiles on two fans offset along the respective range bounding faults of Smith and Mason Valley. The two faults were chosen for study because they have not previously been subject of a slip rate study or large uncertainties are associated with the currently existing estimate.

## Regional Context

### The Fault Bounded Basins of the Northern Walker Lane

The major active faults and physiography of the Walker Lane are shown in **Figure 1**. Smith and Mason valleys are two of a set of seven normal fault-bounded basins arranged in a generally en echelon and left-stepping manner that, for simplicity, we will herein call the Northern Walker Lane (**Figure 1**: the Tahoe, Carson, Smith, Mason, Antelope, Bridgeport and Walker Lake basins). The area also includes the east trending left-lateral Olinghouse fault (e.g. Briggs and Wesnousky 2001) and Carson and Wabuska lineaments. The Carson and Wabuska lineaments are expressed by near-alignment of valleys and mountain ranges and have been considered zones of left slip (Cashman and Fontaine 2000, Rogers 1975).

The normal fault-bounded basins are the most profound and active structural elements in the region between and to the west of the major strike-slip faults of the central and northern Walker Lane. Smith and Mason Valley sit within the central portion of this en echelon arrangement of normal fault bounded basins.

### **Rates and Styles of Fault Slip from Geology**

Earthquake displacements reported in the trenches along the Wassuk, Smith Valley, Carson (Genoa), and Antelope basin-bounding faults are dip-slip (Bormann et al. 2012, Ramelli et al. 1999, Sarmiento 2010, Sarmiento et al. 2011, Wesnousky and Caffee 2011). The steep range fronts, triangular facets, discontinuous and sinuous traces, and consistent presence of scarps showing down-to-the-basin displacement further attest to dip-slip motion on the range-bounding faults. The same is true for the Tahoe, Bridgeport and Mason basins. Geologic observations thus indicate that the horizontal projection of slip along each of the basin bounding faults is dominantly normal to the average strike of the respective faults. Drawing on the summary and analysis of Wesnousky et al. (2012), the horizontal projection of fault slip rate along each of the basin-bounding faults is given and depicted by black arrows adjacent to the sites of the studies in **Figure 2**.

### **Rates and Styles of Fault Slip from Geodesy**

The red vectors in **Figure 2** represent the estimated velocity of each GPS station with respect to the Sierra Nevada and are calculated using the methodology outlined in Hammond et al. (2011). The vectors are consistently oriented to the southeast and increase in magnitude as one progresses northeastward from the Sierra Nevada. The pattern defines to first order a simple right-lateral shear field oriented along the trend of the Walker Lane. The rate of right-lateral strain accumulation between station LANT in the Sierra Nevada and station RAIN about 120 km to the northeast is 5-6 mm/yr (**Figure 2**). By differencing the interpolated velocity field in a 20-30 km transects across each fault, Wesnousky et al. (2012) approximated the fault normal and parallel components of slip rate by differencing the interpolated velocity field in a 20-30 km transect perpendicular to each fault. The calculated rates of fault normal (horizontal extension) and strike-slip are annotated and shown in **Figure 2** with violet and blue arrows, respectively.

### **Geology versus Geodesy across the Region**

Three paths labeled AB, CD, and EF, respectively, are drawn in yellow perpendicular to the shear field in **Figure 2**. Critical to the tenet of this proposal, no faults are intersected by path AB and accordingly no part of the geodetic velocity field may be accounted for with displacement on the major range-bounding faults. Similarly, for paths CD and EF, which do intersect major range-bounding faults, neither geodetic nor geologic rates are of size or orientation to account for the entire geodetic slip budget of 5-6 mm/yr. The amount of geodetically observed deformation that may be accounted for on basin-bounding faults is dependent on the path one follows across the region. Regardless of how the discrepancy is accounted for (crustal rotations likely), the observation points to the importance of knowing well the geologic slip rates of the major basin bounding faults, so it can be known what is the exact proportion of the shear field that can be accounted for by fault slip.

## Methodology

$^{10}\text{Be}$  TCN surface exposure dating samples were collected from the surfaces of the Yerington and Artesia fans in Mason and Smith Valley, respectively. Boulder samples were collected from fans offset by rangebounding faults in each Mason and Smith Valleys. The locations of the faults and fan sites are shown in **Figures 3** and **4**.

Samples were collected from flatter elements of alluvial fan surfaces to reduce the likelihood of sampling boulders significantly affected by sediment shielding. For  $^{10}\text{Be}$  dating we preferentially selected quartz-rich boulders that are 1) large, >50 cm in length (a-axis); 2) tall in height relative to the surrounding land surface (>30 cm exposed) to avoid boulder surfaces that may have been recently shielded by sediment or that could be shielded by snow in the winter. Where large boulders were not available, boulders with the best placement and the largest size were sampled). Additionally, boulders that had a well-developed rock varnish and maintained a hard, resistant surface were favored to try to avoid surfaces that may have experienced significant weathering. We took ~500 g of sample from a high, flat surface on each sampled boulder to a depth of 1-5 cm using a small sledgehammer and chisel. Topographic shielding was

determined by use of inclinometer, taking angle measurements from the sample to the horizon in 10° increments. Images of the Yerington and Artesia fan surfaces are shown in **Figures 5** and **6**, respectively, and representative photos of the rocks sampled on each surface are shown in **Figures 7** and **8**, respectively.

In addition to the boulder samples, a two-meter deep pits was dug into the Yerington alluvial fan complex to collect samples for TCN depth profile analysis (**Figure 9**) We collected one kilogram of sediment (>2 cm particle sizes) at intervals of 30-50 cm with at least four samples per pit

Samples were processed at the Geochronology Laboratories at the University of Cincinnati. Each boulder sample was crushed and sieved to obtain the 250-500 µm grain size fraction. For TCN depth profiles, the samples were sieved to obtain the 250-500 µm grain size fraction. Quartz isolation, dissolution, chromatography, isolation of Be, and preparation of BeO followed the methods of Kohl and Nishiizumi (1992) for all samples; these methods are described in detail in Dortch et al. (2009). Ratios of  $^{10}\text{Be}/^9\text{Be}$  were measured using accelerator mass spectrometry at the Purdue Rare Isotope Measurement Laboratory at Purdue University.

$^{10}\text{Be}$  exposure ages for boulders were calculated using the CRONUS  $^{10}\text{Be}$  -  $^{26}\text{Al}$  exposure age calculator (version 2.2, Balco et al., 2008; Table 1). We use the Lal (1991) and Stone (2000) time-dependent model to discuss and evaluate the  $^{10}\text{Be}$  ages. The Lal (1991) and Stone (2000) time-dependent model uses a  $^{10}\text{Be}$  production rate of  $4.39 \pm 0.37$  atoms  $\text{g}^{-1} \text{yr}^{-1}$  and accounts for  $^{10}\text{Be}$  production rate flux due to temporal changes in the geomagnetic field.

For the depth profiles, an exponential curve was plotted through the TCN concentrations of samples versus depth can then be extrapolated upwards to the surface, thereby constraining the age of the surface (Anderson et al. 1996, Hancock et al. 1999). If there had been significant erosion of the surface, then the depth profile age represents a minimum value, presuming there had been no prior exposure of the sediment to cosmic rays. Depth profiles can also be used to check for prior exposure of the sediment to

cosmic rays, which results in inherited TCNs, by examining the shape of the depth curve for TCN concentrations (e.g., Anderson et al. 1996, Hancock et al. 1999).

Two sets of problems are associated with the application of TCN methods to alluvial fan surfaces. The first set of problems relate to the use of the appropriate scaling models and geomagnetic corrections for  $^{10}\text{Be}$  production to calculate  $^{10}\text{Be}$  ages. We present the TCN ages using five scaling models. The second set of problems relates to geologic factors. These include weathering, exhumation, prior exposure and shielding of the surface by snow and/or sediment.

With the exception of prior exposure to cosmic rays, these factors generally reduce the concentration of TCNs in rock surfaces, which results in an underestimate of the true age of the landforms and may lead to a large spread in apparent exposure ages on a landform. This is particularly so for surfaces are many tens to hundreds of thousands of years old because their surface boulders are generally significantly weathered and/or may have been exhumed from depth during prolonged periods of erosion. Periods of prior exposure of boulders result in an overestimate of the true age of the moraine. Geologic factors often eclipse the problems associated with production rates. To help address the geologic problems multiple sample are collected from the same surface, with the view that the variability of ages on the surface reflects the degree to which these factors have operated, in essential since these geologic factor are stochastic then little variability in ages reflects little geologic influence.

We examined our  $^{10}\text{Be}$  exposure age results using normal distribution (mean and  $1\sigma$ ) to examine the robustness of the dataset and attempt to determine most likely age for each surface. Comparison of dataset mean and  $1\sigma$  values gives a sense of dataset scatter and the most likely age based on range of age results. The uncertainty associated with AMS measurements is given as  $1\sigma$  values, which includes the internal (analytical) and external (analytical and production rate) uncertainty

## **Results of Exposure Dating.**

*Mason Valley*. The TCN surface exposure ages of rocks and profiles are summarized in **Figures 9, 10, 11** and **Table 1**. There is considerable spread of boulder ages, 78-387 ka, on the older surface on the

Yerington alluvial fan (**Figure 11**). The depth profile confirms that the surface must be at least 100 ka. The number of boulders present on the fan surface are very few and thus the locations of the samples were somewhat dictated by where there was a boulder present. The profile age sits within and at the lower end of boulder exposure ages. The younger boulder ages in the distribution are possibly the result of exhumation and/or weathering, which results in an underestimate of the ages. Likewise, we cannot determine whether the older ages in the boulder distribution are the result of inheritance or truly reflect the ages of the surface. The minimum boulder age, the profile age determination, and maximum boulder ages of the surface are thus expressed as 78ka, 103ka, and 387ka, respectively. The profile age falls near the lower bound of the spread in ages. Some support for this lower value may be drawn from the observed soil characteristics observed in the profile pit (**Figures 9a and b**). Previous studies summarized in Koelher and Wesnousky (2011) indicate that soils that exhibit stage II to II+ carbonate development are late middle Pleistocene to late Pleistocene in age (ca. 50–175 ka). The soil observed in the pit exhibits a thin ~10 cm thick Bt horizon and a yet thinner Bk horizon displaying Stage 1+ to II carbonate development. The presence of a Bt horizon provides a firm bound that the soil is greater than 15 ka age because Bt horizons are known not to be present on Lake Lahontan shorelines throughout the region (Adams and Wesnousky 1999). The presence of Stage 1+ to II soil carbonate suggests soil forming processes commenced toward the lower end of the approximate 50-175 ka range. In these regards, we assume a preferred age of the surface equal to 103 ka, and the boulder ages to provide us maximum and minimum bounds on that estimate.

*Smith Valley*: The range-bounding fault displaces the Artesia alluvial fan surface shown in **Figure 6**. The alluvial fan displays 3 distinct surfaces: Oy, Qi, and Qo in order of increasing age (Figure 11). The location and approximate surface exposure ages of boulders sampled from the Artesia fan surface are also shown in **Figure 12**, and summarized in more detail in **Table 1**. Seven samples were taken from the foot and hanging wall surfaces of unit Qi. Large sub angular white and generally unvarnished granitic boulders are abundant on the Qi surface. The Qo surface of the unit is composed of large white unvarnished subangular and angular boulders. The range of boulder ages for the 7 boulders sampled from the Qi surface range from 9-30 ka. The distribution is bimodal with ages clustering around 11 ka and an older group ranging from 18-30 ka. Rather than speculate the role of inheritance of weathering in leading to the

spread and bimodal distribution of ages, we interpret the exposure ages to indicate the Qi fan element is late Pleistocene in age with mean age of  $17 \pm 8$  ka (uncertainty = 1 sigma).

The presence of few boulders on the Qo fan surface limited the site selection of boulders and is in contrast to the ubiquitous number of boulders on the Qi surface. Additionally the Qo surface boulders and gravel are oxidized red in color, in distinct contrast to the white unvarnished boulders on the surface of unit Qi. We interpret the lesser number of boulders on the Qo surface to be in large part due to weathering and gussification over a time period significantly longer than the Qi surface. Boulder ages on Qo range from 16 to 60 ka, and perhaps may be viewed to cluster around 26-34 ka. The large ~22 km scarp appears to have been modified by wave action during the high stand of a lake that filled the valley. A tephra (SGW-SV1-2008) was sampled along a roadcut exposing fine-grained gray lacustrine sediments below the alluvial Qo surface. Statistical analyses performed by the USGS Tephrochronology Project showed the tephra to have a best-matching similarity coefficient of 0.96 with a Pleistocene tephra (~75-80 ka, correlated age range) recovered from Owens Lake in southeast California. The correlated age-range is based on a sedimentation rate curve presented by Bischoff et al. (1997) (Elmira Wan, U.S. Geological Survey, pers. comm.). This observation indicating the presence of the lake ~75-80 ka, the oxidized character of gravel on the Qo surface, and the paucity of boulders on the surface lead us to interpret that the cosmogenic ages are providing a minimum bound on the age of the Qo surface. This interpretation is perhaps enhanced by the observation that most of the boulders present and sampled on the Qo surface are sampled from an element of the unit that is between and near two strands of the fault, where one might expect slope degradation processes to be greatest.

### **Slip Rates and Discussion**

*Mason Valley.* A profile across the faulted Yerington moraine shows it to display ~10 m of vertical separation. It is to our knowledge the only fan element clearly offset along the entire Mason Valley range front. The minimum boulder age, the preferred profile age determination, and maximum boulder ages of the surface determined from our analysis are 78ka, 103ka, and 387ka, respectively. Dividing the vertical offset of 10 m by these ages yields an estimated vertical separation rate of  $0.097^{+0.031}_{-0.072}$  mm/yr. Assuming displacement occurs on a 60° dipping fault, the preferred values of fault slip rate and extension are .112 mm/yr and 0.056 mm/yr. This is the first geologic estimate of fault slip rate in Mason Valley. The

extension rate suggested by the geodetic analysis put forth in Wesnousky et al. (2012) and shown in Figure 2 is 0.7-0.9 mm/yr. The geologic rate in this case is significantly less than predicted by our geological analysis. The geodetic rate was calculated at a site many kilometers to the south which may account for some of the difference. Further geodetic analysis will be required to assess the possibility.

*Smith Valley.* Numerous profiles were constructed and measured across the Qi surface of the Artesia fan in Smith Valley and each is shown in **Figure 12**. The Qi surface is broken by two splays of the fault and the measurements of cumulative vertical separation across the scarps range when taken together indicate about 10 m of cumulative vertical separation. The values of vertical separation for each profile are annotated next to the profile in **Figure 12**. Dividing the 10 meter vertical separation by the age of  $17 \pm 8$  ka age of the surface determined from exposure dating places the vertical separation rate at about  $0.59^{+0.52}_{-0.19}$  mm/yr. Following the same approach as for Mason Valley, assuming displacement occurs on a  $60^\circ$  dipping fault, the preferred values of fault slip rate and extension are 0.68 mm/yr and 0.58 mm/yr, respectively. The extension rate suggested by the geodetic analysis put forth in Wesnousky et al. (2012) and shown in Figure 2 is 0.7-1.2 mm/yr. Unlike in Mason Valley, the estimated extension rate from geological analysis is, within uncertainties, about the same as estimated from the geodesy.

We will elaborate further on these results as they are prepared for publication in a professional journal.

## References.

- Adams, K. D., and S. G. Wesnousky (1999). The Lake Lahontan highstand: age, surficial characteristics, soil development, and regional shoreline correlation, *Geomorphology* **30** 357-392.
- Anderson, R. S., J. L. Repka, and G. S. Dick (1996). Explicit treatment of inheritance in dating depositional surfaces using in situ Be-10 and Al-26, *Geology* **24** 47-51.
- Bormann, J. M., B. E. Surpless, M. W. Caffee, and S. G. Wesnousky (2012). Holocene Earthquakes and Late Pleistocene Slip-Rate Estimates on the Wassuk Range Fault Zone, Nevada, *Bulletin of the Seismological Society of America* **102** 1884-1891.
- Briggs, R. W., and S. G. Wesnousky (2001). Paleoseismic evidence for repeated Holocene earthquakes on the Olilnghouse fault zone, western Nevada, *EOS Transaction (supplement)* **82** F935.
- Cashman, P. H., and S. A. Fontaine (2000). Strain partitioning in the northern Walker Lane, western Nevada and northeastern California, *Tectonophysics* **326** 111-130.

- Hammond, W. C., G. Blewitt, and C. Kreemer (2011). Block modeling of crustal deformation of the northern Walker Lane and Basin and Range from GPS velocities, *Journal of Geophysical Research-Solid Earth* **116**.
- Hancock, G. S., R. S. Anderson, O. A. Chadwick, and R. C. Finkel (1999). Dating fluvial terraces with Be-10 and Al-26 profiles: application to the Wind River, Wyoming, *Geomorphology* **27** 41-60.
- Koehler, R. D., and S. G. Wesnousky (2011). Late Pleistocene regional extension rate derived from earthquake geology of late Quaternary faults across the Great Basin, Nevada, between 38.5° and 40°N latitude, *Bulletin of the Geological Society of America* **123** 631-650.
- Kohl, C. P., and K. Nishiizumi (1992). Chemical isolation of quartz for measurement of insitu-produced cosmogenic nuclides, *Geochimica Et Cosmochimica Acta* **56** 3583-3587.
- Lal, D. (1991). Cosmic-ray labeling of erosion surfaces - insitu nuclide production-rates and erosion models, *Earth and Planetary Science Letters* **104** 424-439.
- Ramelli, A. R., J. W. Bell, C. M. dePolo, and J. C. Yount (1999). Large-magnitude, late Holocene earthquakes on the Genoa Fault, west-central Nevada and eastern California, *Bulletin of the Seismological Society of America* **89** 1458-1472.
- Rogers, D. K. (1975). The Carson Lineament - Its influence on recent left-lateral faulting near Carson City, Nevada, *Geological Society of America Abstracts with Programs*. **7** 1250.
- Sarmiento, A. C. (2010). Earthquake recurrence and modes of deformation in the central and northern Walker Lane: observations from paleoseismic trenches across the Carson and Sierra Nevada Range fronts, in *Geological Sciences*, University of Nevada, Reno.
- Sarmiento, A. C., S. G. Wesnousky, and J. M. Bormann (2011). Paleoseismic trenches across the Carson and Sierra Nevada range fronts in Antelope Valley, California and Reno, Nevada, *Bulletin of Seismological Society of America* **101** 2542-2549.
- Stone, J. O. (2000). Air pressure and cosmogenic isotope production, *Journal of Geophysical Research-Solid Earth* **105** 23753-23759.
- Wesnousky, S. G., J. M. Borman, C. Kreemer, W. C. Hammond, and J. N. Brune (2012). Neotectonics, geodesy, and seismic hazard in the Northern Walker Lane of Western North America: Thirty kilometers of crustal shear and no strike-slip, *Earth and Planetary Science Letters* **329-330** 133-140.
- Wesnousky, S. G., and M. W. Caffee (2011). Rangebounding normal fault of Smith Valley, Nevada: Limits on age of last surface rupture earthquake and late Pleistocene rate of displacement, *Bulletin of Seismological Society of America* **101** 1431-1437.

		(°N)	(°W)	(m)	(cm)			(mg)	(µg/g)		(ka)	(ka)	(ka)	(ka)	(ka)			
<b>Mason Valley</b>																		
Upper Yerington fan surface																		
MVS1	Granite	38.9669	119.2012	1424	27022090	1	0	1.0000	14.5495	0.3508	1025.5	28.604 ± 0.807	47.235 ± 1.334	387.2 ± 12.4 (40.1)	383.5 ± 51.3	377.3 ± 50.1	370.1 ± 41.7	368.0 ± 35.9
MVS2	Granodiorite	38.9661	119.2019	1430	1008525	3	0	1.0000	24.8750	0.3498	1025.5	10.593 ± 0.254	10.208 ± 0.2445	80.4 ± 2.0 (7.4)	78.7 ± 9.7	77.6 ± 9.5	76.3 ± 7.9	75.7 ± 6.8
MVS3	Granodiorite	38.9660	119.2034	857	804025	2	0	1.0000	13.1176	0.3497	1025.5	7.020 ± 0.228	12.824 ± 0.416	156.8 ± 5.3 (15.1)	156.2 ± 19.9	154.4 ± 19.5	151.7 ± 16.4	147.3 ± 13.8
MVS4	Granodiorite	38.9653	119.2028	1431	1105015	2	0	1.0000	3.9100	0.3505	1025.5	1.621 ± 0.075	9.878 ± 0.351	77.7 ± 2.8 (7.4)	76.0 ± 9.5	75.0 ± 9.4	73.7 ± 7.9	73.1 ± 6.8
M1 - P1 - 20	Fanglomerate	38.9669	119.2012	1425	Sand	5	20 ± 5	1.0000	17.2417	0.3494	1023.2	6.899 ± 0.075	9.559 ± 1.042	-	-	-	-	-
M1 - P1 - 40	Fanglomerate	38.9669	119.2012	1425	Sand	5	40 ± 5	1.0000	14.6023	0.3510	1023.2	7.847 ± 0.068	1.290 ± 1.120	-	-	-	-	-
M1 - P1 - 100	Fanglomerate	38.9669	119.2012	1425	Sand	5	100 ± 5	1.0000	14.5966	0.3504	1023.2	3.919 ± 0.055	6.434 ± 0.908	-	-	-	-	-
M1 - P1 - 160	Fanglomerate	38.9669	119.2012	1425	Sand	5	160 ± 5	1.0000	17.7308	0.3500	1023.2	2.241 ± 0.0502	3.025 ± 0.677	-	-	-	-	-
<b>Smith Valley</b>																		
Artesia Fan - oldest surface																		
SF1	Granite	38.8908	119.4158	1494	1008055	1	0	0.9920	16.7696	0.3510	1025.5	2.486 ± 0.098	3.566 ± 0.141	26.2 ± 1.0 (2.5)	26.6 ± 3.3	26.2 ± 3.3	26.0 ± 2.8	25.5 ± 2.4
SF2	Granodiorite	38.8909	119.4163	1497	603530	4	0	0.9913	15.3773	0.3515	1025.5	1.365 ± 0.077	2.139 ± 0.120	16.1 ± 0.9 (1.7)	16.7 ± 2.2	16.5 ± 2.2	16.4 ± 1.9	15.9 ± 1.6
SF3	Granite	38.8903	119.4158	1491	709020	1	0	0.9923	7.2053	0.3516	1025.5	1.427 ± 0.013	4.771 ± 0.418	35.3 ± 3.1 (4.4)	35.0 ± 5.2	34.5 ± 5.1	34.1 ± 4.5	33.7 ± 4.1
Artesia Fan - oldest surface (Wenousky and Caffee, 2011)																		
CWL-2	Granite	38.8907	119.4150	1480	655025	2	0	0.9922	-	-	-	3.74 ± 0.191	28.0 ± 1.4 (2.8)	28.3 ± 3.7	27.9 ± 3.6	27.7 ± 3.1	27.2 ± 2.7	
CWL-3	Granite	38.8907	119.4148	1470	1109035	2	0	0.9922	-	-	-	4.69 ± 0.324	35.5 ± 2.5 (4.0)	35.2 ± 4.9	34.8 ± 4.8	34.4 ± 4.2	33.9 ± 3.7	
CWL-4	Granite	38.8907	119.4148	1480	807060	3	0	0.9933	-	-	-	7.90 ± 0.427	60.1 ± 3.3 (6.2)	59.0 ± 7.8	58.2 ± 7.6	57.1 ± 6.5	56.7 ± 5.8	
Artesia Fan - younger surface																		
SF4	Granite	38.8892	119.4164	1494	17010030	2	0	0.9929	31.2170	0.3507	1025.5	3.147 ± 0.025	2.423 ± 0.193	17.9 ± 1.4 (2.1)	18.5 ± 2.6	18.3 ± 2.6	18.2 ± 2.3	17.7 ± 2.1
SF5	Granite	38.8892	119.4165	1494	1508025	1	0	0.9929	25.1032	0.3511	1023.2	1.386 ± 0.018	1.326 ± 0.175	9.7 ± 1.3 (1.5)	10.2 ± 1.8	10.2 ± 1.8	10.0 ± 1.6	9.7 ± 1.5
SF6	Granite	38.8893	119.4171	1500	18514065	2	0	0.9917	19.8977	0.3519	1025.5	3.331 ± 0.011	4.044 ± 0.159	29.9 ± 1.0 (2.8)	30.0 ± 3.7	29.6 ± 3.7	29.3 ± 3.1	28.9 ± 2.6
Artesia Fan - lower younger surface																		
SF8	Granite	38.8892	119.4149	1468	22016530	2	0	0.9950	29.7777	0.3501	1023.2	3.899 ± 0.026	3.134 ± 0.211	23.6 ± 1.6 (2.6)	24.1 ± 3.3	23.8 ± 3.2	23.6 ± 2.8	23.1 ± 2.5
SF9	Granite	38.8892	119.4148	1472	1156535	2	0	0.9940	27.3961	0.3515	1023.2	3.471 ± 0.034	3.049 ± 0.295	22.9 ± 2.2 (3.0)	23.4 ± 3.6	23.1 ± 3.5	22.9 ± 3.2	22.4 ± 2.9
SF10	Granite	38.8894	119.4145	1458	959025	2	0	0.9939	21.6136	0.3507	1025.5	1.273 ± 0.019	1.417 ± 0.214	10.7 ± 1.6 (1.9)	11.3 ± 2.2	11.2 ± 2.2	11.1 ± 2.0	10.7 ± 1.9
SF11	Granite	38.8888	119.4142	1450	1307055	5	0	0.9963	22.2842	0.3502	1025.5	0.969 ± 0.011	1.045 ± 0.117	8.1 ± 0.9 (1.2)	8.5 ± 1.4	8.5 ± 1.4	8.3 ± 1.2	8.0 ± 1.1

\*Constant (time-invariant) local production rate based on Lal (1991) and Stone (2000). A sea level, high-latitude value of  $4.5 \pm 0.3$  at  $^{10}\text{Be g}^{-1}$  quartz was used.

\*Constant (time-invariant) local production rate based on Heisinger et al. (2002a,b).

\*A density of  $2.7 \text{ g cm}^{-3}$  was used for all surface samples.

\*Isotope ratios were normalized to  $^{10}\text{Be}$  standards prepared by Nishizumi et al. (2007) with a value of  $2.85 \times 10^{-10}$  and using a  $^{10}\text{Be}$  half life of  $1.36 \times 10^6$  years.

\*Uncertainties are reported at the 1 $\sigma$  confidence level. A denudation rate of  $0 \text{ mm/a}$  is used in the age calculation.

\*A mean blank  $^{10}\text{Be}/^{9}\text{Be} = 2.75 \pm 0.74 \times 10^{-11}$  was used to correct for background for all samples except SF10 and 11 and Well-1 that had a blank of  $1.25 \pm 0.61 \times 10^{-15}$ .

\*Propagated uncertainties include error in the blank, carrier mass (1%), and counting statistics.

\*Uncertainty is expressed as internal and external (in parenthesis).

\*Propagated error in the model ages include a 6% uncertainty in the production rate of  $^{10}\text{Be}$  and a 4% uncertainty in the  $^{10}\text{Be}$  decay constant.

\*Beryllium-10 model ages were calculated with the CRONUS-Earth online calculator, version 2.2 (Balco et al., 2008; <http://hess.ess.washington.edu/>).

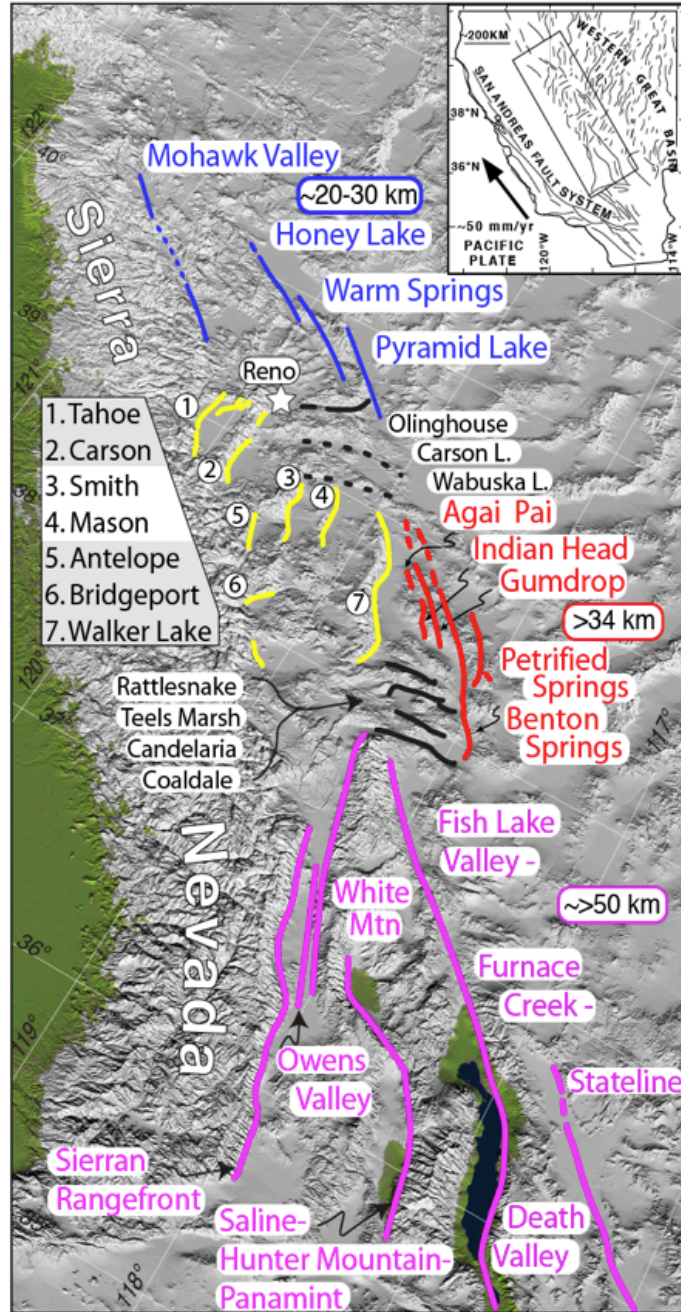


Figure 1. Smith and Mason valleys sit within an en echelon arrangement of major structural basins bounded by active faults (yellow lines) that sit between and east of the strike-slip faults of the central (red) and northern Walker (blue) lane. Values of cumulative right-slip (km) across each the southern (magenta), central (red), and northern (blue) Walker Lane fault systems are annotated and adapted from summary of Wesnousky (2005a). East-west striking left-lateral faults (solid) and structural lineaments (dashed) are black. Rectangle in inset shows location in context of San Andreas and Western Great Basin fault systems. Location of Reno shown by star.

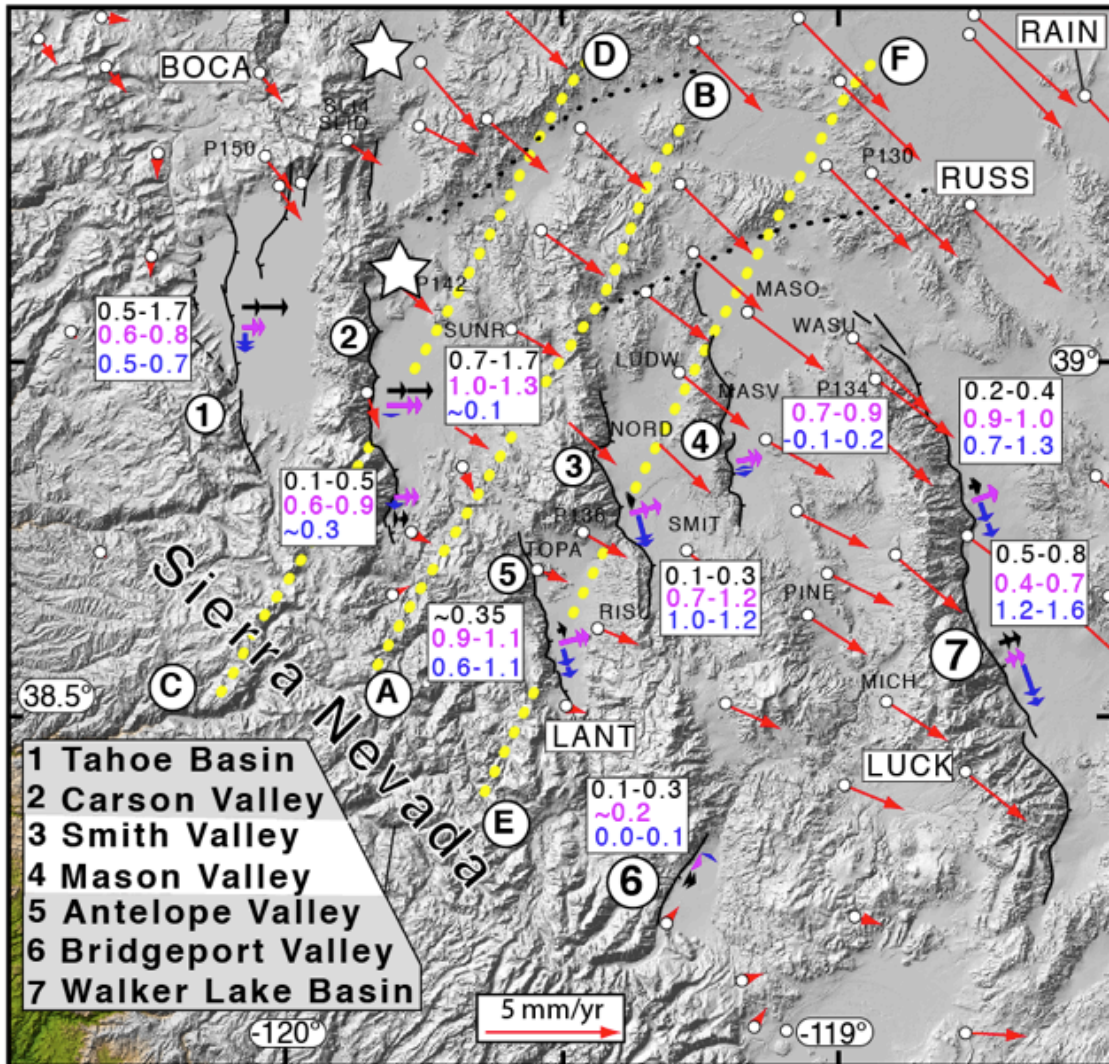


Figure 2. Physiographic and fault map shows location of Smith and Mason valleys and other major structural basins (numbered), active basin-bounding faults (thick black lines), and geodetic displacement field (red arrows) in northern Walker Lane. Shown in white boxes are geologically determined values of fault-normal extension (black-upper text), geodetic estimates of fault-normal extension (magenta-middle text) and geodetic estimates of fault-parallel strike-slip (blue-lower text) rates along each of the basin bounding faults. Two-headed arrows schematically show ranges of same values and correspond in arrangement and color to the values in boxes. The geologically determined extension rate arrows are placed adjacent to the sites of studies except for Lake Tahoe where the estimate is an average value across several submarine faults. Dotted (yellow) lines define paths AB, CD, and EF discussed in text. Stars are the center of Reno and Carson City urban areas.



Figure 3. Sketch of active fault traces and Quaternary deposit along the western edge of Mason Valley. Location of Yerington fan is labeled. Location of Mason Valley shown in Figure 2.





*Figure 5. Aerial photograph of Yerington alluvial fan sampled for TCN analysis. See Figure 3 for location.*



*Figure 6. Oblique aerial photograph of Artesia alluvial fan complex in Smith Valley sampled for TCN analysis. See Figure 4 for location.*

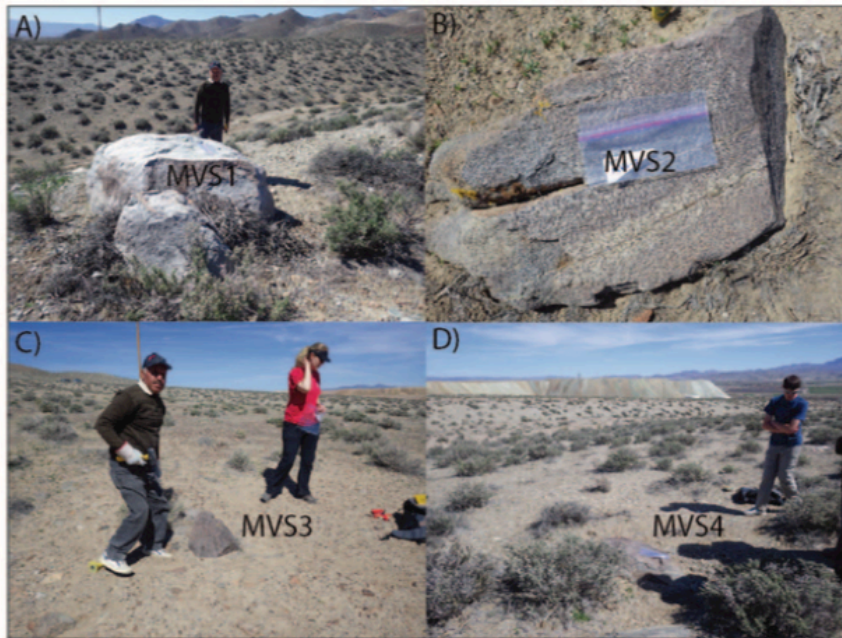


Figure 7. Views of boulders sampled on the Yerington alluvial fan complex (Figure 5) in Mason Valley (Figure 3). The samples are numbered SF1 through SF11.



Figure 8. Views of boulders sampled on the Artesia alluvial fan complex (Figure 6) in Smith Valley (Figure 4). The samples are numbered MVS1 Through MVS4

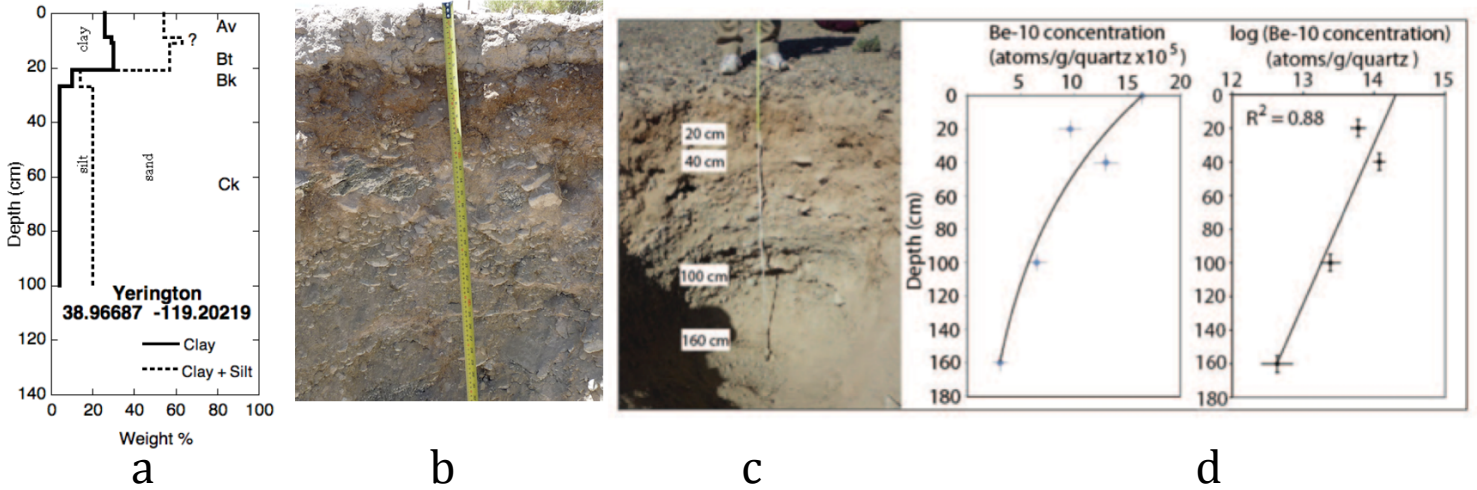


Figure 9. (a) Soil texture profile of pit wall shown in (b) and (c) from which samples were collected to construct  $^{10}\text{Be}$  profiles shown in (d). The depth profiles are consistent with the fan surface being stabilized and abandoned about  $\sim 100\text{ky}$  years ago. The 100 ky estimate is on the same order or viewed by the author as perhaps a bit greater than expected for the observed soil development that displays a moderate Bt horizon thickness and a Bk horizon that displays stage 2 carbonate at best.

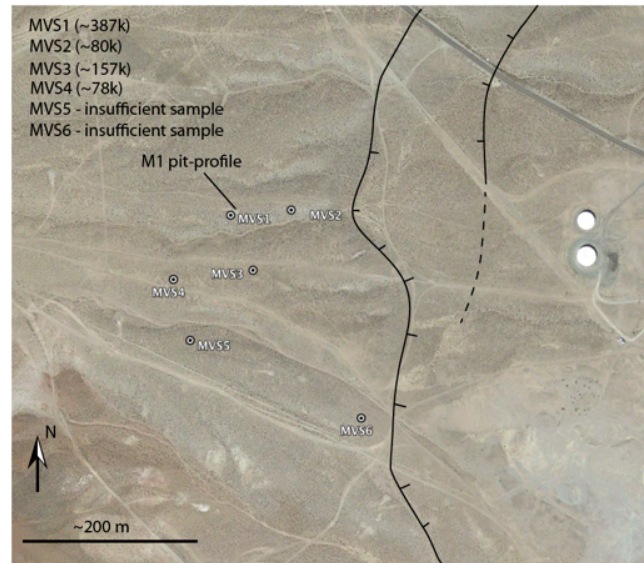


Figure 10. The location of the cosmogenic depth profile shown in Figure 9 and location and  $^{10}\text{Be}$  ages of boulders sampled from the surface of the fan. An additional airphoto image of this site is shown in Figure 5.

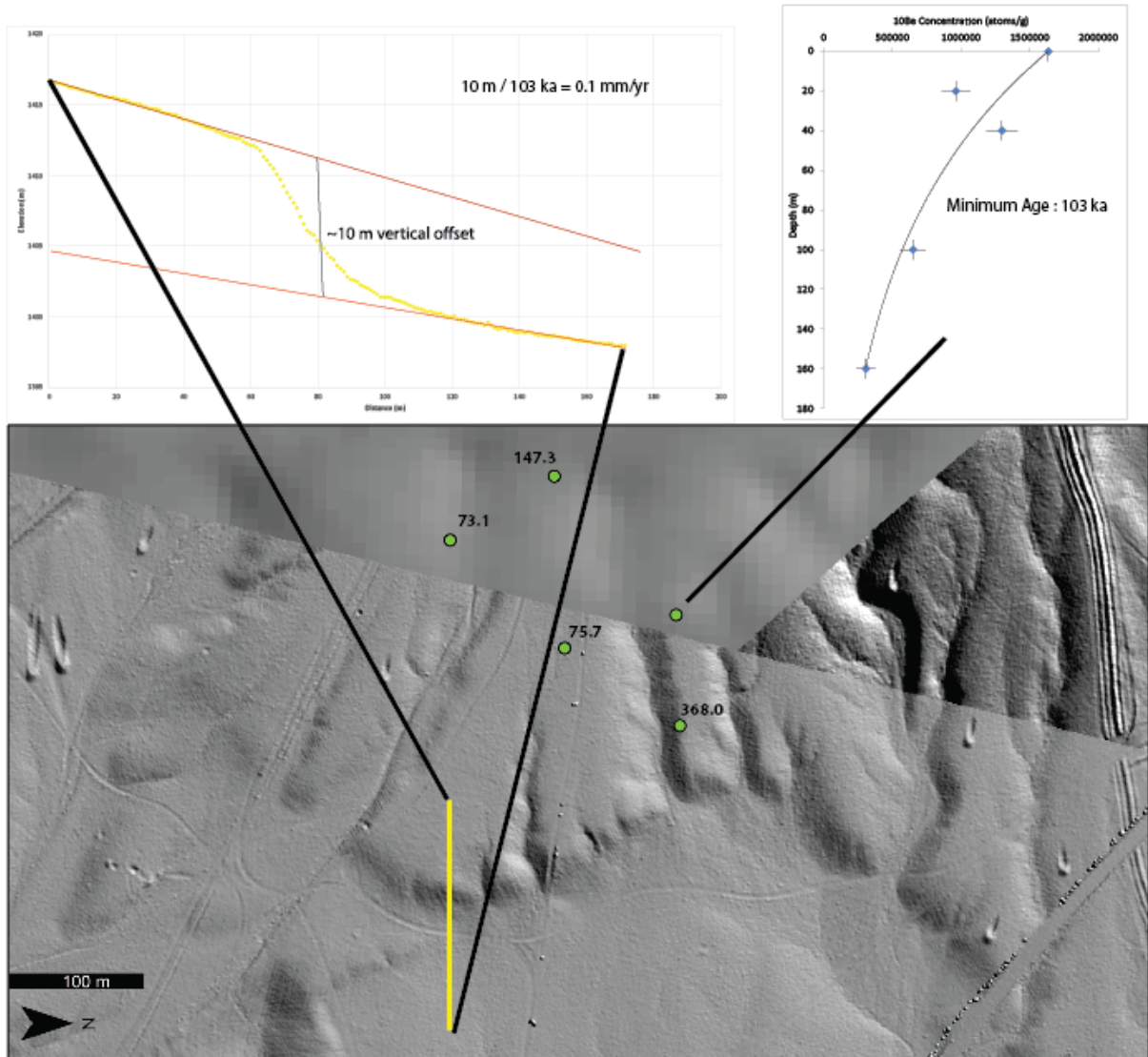


Figure 11. Location and plot of profile across the same Yerington fan shown in Figure 10 indicates surface is vertically offset about 10 m. When divided by the age of the surface indicated by the cosmogenic profile (upper right), the observations yield a best estimate of the vertical slip rate to equal  $\sim 0.1 \text{ mm/yr}$ . The uncertainty associated with the scatter in exposure ages for small boulders collected on the surface are discussed in text.

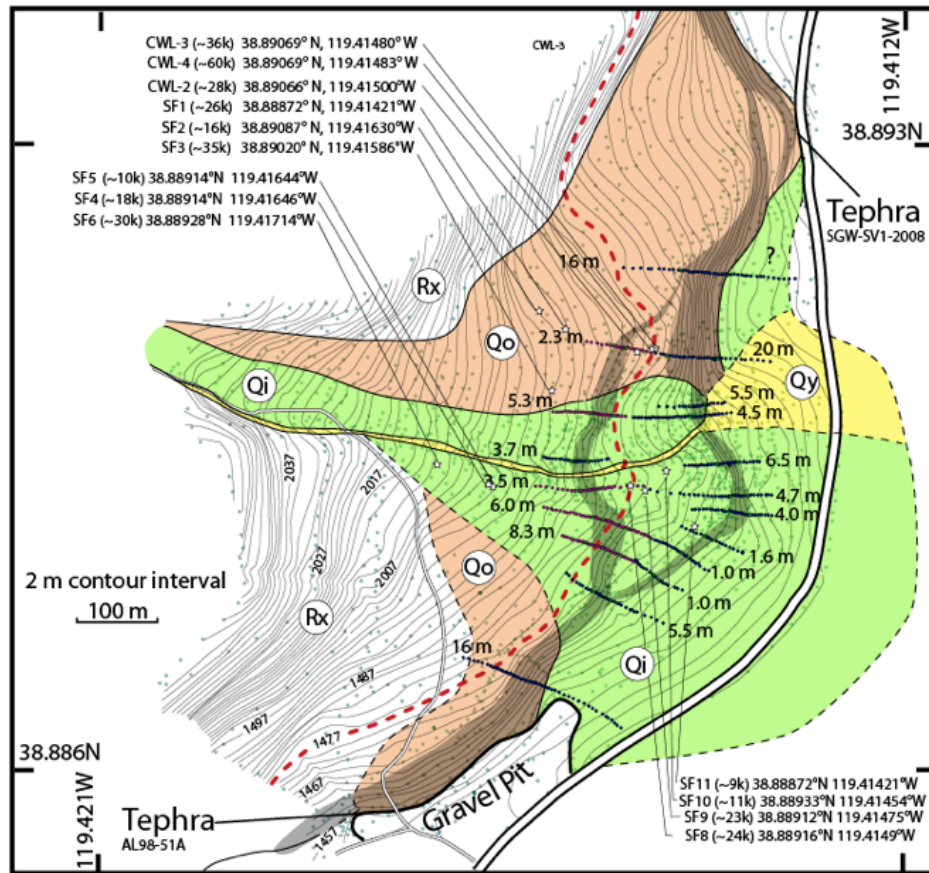


Figure 12. Locations and surface exposure ages of boulders sampled on the Artesia fan. The fault scarp is shaded and values annotated in meters are measured vertical separations across the scarps. Vertical separations on the youngest (green) element of the fan reach to ~10m at their maximum. The boulder ages range from 10 to 30 k. Dividing the offset by the range of ages leads to bound on the vertical separation rate of 0.33 to 1 mm/yr. Lewis needs to comment on how best to handle age range of boulders and I then need to convert to fault slip rate and extension rate to compare to geodesy. The tephra (SGW-SV1-2008) was sampled along a roadcut exposing fine-grained gray lacustrine sediments below the alluvial Qo surface. Statistical analyses performed by the USGS Tephrochronology Project showed the tephra to have a best-matching similarity coefficient of 0.96 with a Pleistocene tephra (~75-80 ka, correlated age range) recovered from Owens Lake in southeast California. The correlated age-range is based on a sedimentation rate curve presented by Bischoff et al. (1997) (Elmira Wan, U.S. Geological Survey, pers. comm.).